

First principles prediction of the valley Hall effect in ScBrCl monolayer

Xiang Yu(于翔), Ping Li(李萍), and Chang-Wen Zhang(张昌文)

Citation: Chin. Phys. B, 2025, 34 (**4**): 047305. DOI: 10.1088/1674-1056/adbacb
Journal homepage: http://cpb.iphy.ac.cn; http://iopscience.iop.org/cpb

What follows is a list of articles you may be interested in

Gate-field control of valley polarization in valleytronics

Ting-Ting Zhang(张婷婷), Yilin Han(韩依琳), Run-Wu Zhang(张闰午), and Zhi-Ming Yu(余智明)
Chin. Phys. B, 2024, 33 (**6**): 067303. DOI: 10.1088/1674-1056/ad401a

Anomalous valley Hall effect in two-dimensional valleytronic materials

Hongxin Chen(陈洪欣), Xiaobo Yuan(原晓波), and Junfeng Ren(任俊峰)
Chin. Phys. B, 2024, 33 (**4**): 047304. DOI: 10.1088/1674-1056/ad1c59

Recent progress on valley polarization and valley-polarized topological states in two-dimensional materials

Fei Wang(王斐), Yaling Zhang(张亚玲), Wenjia Yang(杨文佳), Huisheng Zhang(张会生), and Xiaohong Xu(许小红)
Chin. Phys. B, 2024, 33 (**1**): 017306. DOI: 10.1088/1674-1056/ad0713

Single-layer intrinsic 2H-phase LuX_2 (X = Cl, Br, I) with large valley polarization and anomalous valley Hall effect

Chun-Sheng Hu(胡春生), Yun-Jing Wu(仵允京), Yuan-Shuo Liu(刘元硕), Shuai Fu(傅帅),Xiao-Ning Cui(崔晓宁), Yi-Hao Wang(王易昊), and Chang-Wen Zhang(张昌文)
Chin. Phys. B, 2023, 32 (**3**): 037306. DOI: 10.1088/1674-1056/ac89d6

Spin- and valley-polarized Goos-Hänchen-like shift in ferromagnetic mass graphene junction with circularly polarized light

Mei-Rong Liu(刘美荣), Zheng-Fang Liu(刘正方), Ruo-Long Zhang(张若龙), Xian-Bo Xiao(肖贤波), and Qing-Ping Wu(伍清萍)
Chin. Phys. B, 2023, 32 (**3**): 037301. DOI: 10.1088/1674-1056/ac89e2

First principles prediction of the valley Hall effect in ScBrCl monolayer

Xiang Yu(于翔), Ping Li(李萍), and Chang-Wen Zhang(张昌文)†

School of Physics and Technology, Institute of Spintronics, University of Jinan, Jinan 250022, *China*

(Received 19 September 2024; revised manuscript received 7 February 2025; accepted manuscript online 27 February 2025)

Two-dimensional (2D) ferrovalley materials with valley-dependent Hall effect have attracted great interest due to their significant applications in spintronics. In this paper, by using first-principles computational simulations, we predict that the ScBrCl monolayer is a 2D ferrovalley material with valley-dependent multiple Hall effects. After calculations, we found that the ScBrCl monolayer has excellent thermodynamic stability and kinetic stability, and has a high magnetic transition temperature. When the magnetization direction is turned from in-plane to out-of-plane, a large valley polarization of 44 meV can be generated. In particular, under 5.1%–5.3% tensile strain conditions, ScBrCl monolayer can achieve quantum anomalous Hall effect, and further prove its existence through non-zero Chern number and non-trivial edge state. Our discovery enriches the research on valley-dependent Hall effect and promotes the potential application of 2D Janus monolayer in valley electronics.

Keywords: valley polarization, valley-dependent Hall effect, band structure, spintronics

PACS: 73.43.–f, 75.50.Pp, 85.75.–d, 71.15.Mb

DOI: 10.1088/1674-1056/adbacb **CSTR:** 32038.14.CPB.adbacb

1. Introduction

Two-dimensional (2D) materials have very specific physical properties and potential applications of new nanodevices in the future.[1–3] Because it is one-dimensional lower than common three-dimensional (3D) materials, 2D materials often exhibit significant differences in properties compared to their corresponding materials, resulting in novel physical phenomena.[4–6] Generally, crystal materials have four basic degrees of freedom, namely, lattice, orbit, charge, and spin, in 2D materials, then people discovered new valley degree of freedom.[7,8] In recent years, the degree of freedom and related operations in valleys have become an increasing topic of discussion.[9–11] It is found that valley degrees of freedom can be coupled to spin degrees of freedom, and after spin-valley coupling, numerous new quantum effects have been discovered, for instance, valley Hall effect,[12–17] valley spin Hall effect, valley quantum anomalous Hall effect (VQAHE), and layer-valley Hall effect.[18–23] Transition metal elements contain localized d-orbital electrons, in which case the coupling effect is more pronounced, and the coupling effect increases with the decrease of size. Therefore, 2D transition metal materials provide a good platform to study properties related to charge, spin, topology, and valley covariant effects.[24]

In 2D hexagonal lattice materials, the energy extremes of the valence band and conduction band appear at the K and K' points, respectively, thus two valleys are formed, which can be used for valley related device design.[25–27] When people encode and process information, they can also rely on valley degrees of freedom.[28,29] The phenomenon known as spin-valley locking refers to the fact that the energy valleys at K and K' in the Brillouin region have the same energy but opposite symbols by reason that the inversion symmetry is broken and the spin–orbit coupling (SOC) is produced. The result is that charged carriers in two opposite valleys are selectively excited by photons with left- and right-handed circular polarization. Furthermore, if the system further breaks the time reversal symmetry, the valley polarization occurs. Many methods of breaking symmetry have been developed, such as static magnetic fields, magnetic doping, and magnetic proximity effects, as well as dynamic optical pumping technique.[26,30–34] Due to the difficulties in the practical implementation of such materials and their inherent limitations, their application in the field of valley electronics has been hindered. It is expected to find materials with spontaneous valley polarization, this is the so-called ferrovalley (FV).[35] Therefore, exploring FV materials is beneficial for promoting the development of spintronics and valley electronics.[36–38] Recently, YX_2 (X = I, Br, and Cl) monolayer has been found to be 2D ferrovalley semiconductor (FVS) with both dynamic and thermal stabilities, while exhibits large spontaneous valley polarization. Subsequently, its derivative YBrI was predicted to be an FV material that can induce valley polarization under out-of-plane magnetic anisotropy.[39,40]

In this paper, we discuss the stability, magnetic and electronic properties of ScBrCl monolayer. The results show that ScBrCl is a Janus ferromagnetic material with good dynamic,

†Corresponding author. E-mail: ss_zhangchw@ujn.edu.cn

© 2025 Chinese Physical Society and IOP Publishing Ltd. All rights, including for text and data mining, AI training, and similar technologies, are reserved.

mechanical and thermal stabilities. The ground state magnetization direction of ScBrCl monolayer is in-plane magnetization. After the direction of magnetization is reversed, the electronic properties of ScBrCl monolayer are changed, and resulting in a significant valley polarization phenomenon. When strain is applied to ScBrCl monolayer, a noteworthy topological phase transition can occur, leading to the VQAHE. Our findings contribute to further expanding our understanding of 2D FV materials and better applying them to spintronics.

2. Computational methods

We use density functional theory (DFT)[41,42] and projector-augmented-wave (PAW) potentials and plane wave foundations to calculate the first principle calculations of spin polarization, the above is implemented in the Vienna *Ab-initio* Simulation Package (VASP) code.[43,44] The exchange–correlation functional is processed through the generalized gradient approximation of Perdew, Burke, and Ernzerhof (PBE-GGA).[45,46] The cutoff energy of 500 eV is used as the convergence criterion for energy and force are chosen as 10^{-7} eV and 0.001 eV/Å, respectively. The GGA+U method[47,48] is used to describe the strong correlation correction of Sc-3d orbital, and 3 eV is selected as the U parameter without special explanation. We use the $15 \times 15 \times 1$ Γ-centered Monkhorst–Pack grid when sampling the Brillouin region.

Based on finite-displacement supercell method, the phonon dispersion is calculated in a $5 \times 5 \times 1$ supercell using phonopy code.[49] In the canonical ensemble, based on the density of functional perturbation theory,[50,51] *Ab initio* molecular dynamics (AIMD) simulations[52] are performed on $4 \times 4 \times 1$ supercells with a temperature controlled at 300 K. The Berry curvatures of ScBrCl monolayer are calculated directly from the calculated wave functions, which is implemented in the VASPBERRY code.[53] In addition, we use the WANNIER 90 software package[54,55] to construct the maximum localized Wannier function (MLWF) and the edge state and anomalous Hall conductivity (AHC) are calculated using the WANNIERTOOLS subroutine.[56,57]

3. Results and discussion

3.1. Structure and stability

Similar to monolayer MoSSe,[58] the ScBrCl monolayer has no spatial inversion symmetry, which is composed of Cl–Sc–Br sandwich layer. In ScBrCl monolayer, each Sc atom is connected with three Br and three Cl atoms, showing a triangular prism. Figures 1(a) and 1(b) show the atomic structure of ScBrCl monolayer under two different perspectives. After calculations, the optimized lattice constant is 3.67 Å, and the space group is $P3m1$. The formation energy (E_{form}) can be used to estimate the feasibility of experimentally synthesizing ScBrCl, which is expressed as

$$E_{\text{form}} = \frac{E_{\text{Sc}} + E_{\text{Br}} + E_{\text{Cl}} - E_{\text{ScBrCl}}}{3}, \tag{1}$$

where E_{ScBrCl} is the energy of ScBrCl monolayer, E_{Sc}, E_{Br}, and E_{Cl} are the energies of Sc, Br, and Cl atoms in their most stable 3D structure, respectively. Subsequently, we calculate its cohesive energy E_{coh}, which is expressed as

$$E_{\text{coh}} = \frac{\mu_{\text{Sc}} + \mu_{\text{Br}} + \mu_{\text{Cl}} - E_{\text{ScBrCl}}}{3}. \tag{2}$$

Here, μ_{Sc}, μ_{Br}, and μ_{Cl} represent the energies of single isolated Sc, Br, and Cl atoms. The cohesive energy is found to be 2.50 eV per atom, meaning that the element phase has good thermodynamic stability.

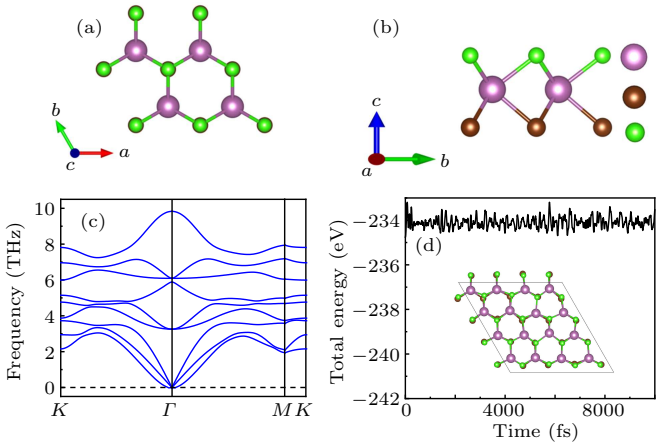


Fig. 1. (a) and (b) Top and side views of ScBrCl monolayer structure, respectively, (c) its phonon dispersion curve, (d) the AIMD simulation at 300 K for ScBrCl monolayer.

As shown in Fig. 1(c), the phonon dispersion shows that there is no virtual frequency in any branch of the entire Brillouin region, which ensures the dynamic stability of ScBrCl monolayer. At a temperature of 300 K, AIMD simulations with a duration of 10 ps is performed. As shown in Fig. 1(d), by observing the final configuration of ScBrCl monolayer after the simulation, it can be seen that the monolayer structure has not been significantly damaged, confirming that ScBrCl monolayer has good thermal stability at room temperature. Simultaneously, the elastic tensor matrices are calculated to be $C_{11} = 39.44$ N/m > 0, and $C_{11} - C_{12} = 28.29$ N/m > 0. It is found that it accords with the Born–Huang criterion,[59] which proves the mechanical stability. Together, these results demonstrate the feasibility of synthesizing ScBrCl monolayers in the laboratory.

3.2. Magnetic properties

We calculated the magnetic properties of ScBrCl monolayer and found that the magnetic moment per ScBrCl monolayer is 1.0 μ_{B}, which is mainly derived from Sc atoms. We also calculated the energies of two configurations by one rectangular supercell, AFM (E_{AFM}) and FM (E_{FM}), as shown in

Fig. S1 of the supporting materials. The energy difference ($\Delta E = E_{\rm AFM} - E_{\rm FM}$) is 99.39 meV, which indicates that the most stable magnetic configuration for ScBrCl monolayer is FM state. When considering the SOC effect, it is very important to determine the direction of magnetization, so we calculate the magnetic anisotropy energy (MAE). The MAE can be expressed as

$$E_{\rm MAE} = E_{[100]} - E_{[001]}, \tag{3}$$

where $E_{[100]}$ and $E_{[001]}$ represent the total energy of ScBrCl monolayer when the magnetic moment direction is along in-plane and out-of-plane, respectively. The MAE is calculated to be -50.19 meV, which indicates that the easy magnetization axis is along in-plane. So, ScBrCl monolayer is considered as one 2D XY magnet. By overcoming the potential barrier of 50.19 meV, we can adjust the magnetization direction from in-plane to out-of-plane.

In order to ensure that the ScBrCl monolayer has a better application, the magnetic transition temperature should be greater than or equal to the room temperature. For the 2D XY magnets[60] with a typical triangular lattice structure, when the temperature reaches the critical temperature $T_{\rm C}$, the Berezinskii–Kosterlitz–Thouless (BKT) transition will take place, which can be calculated using the following formula:[61,62]

$$T_{\rm C} = 1.335\frac{J}{k_{\rm B}}. \tag{4}$$

The $k_{\rm B}$ is the Boltzmann constant, and the nearest neighbor exchange parameter J is expressed as

$$J = \frac{E_{\rm AFM} - E_{\rm FM}}{8S^2}. \tag{5}$$

Here, the energies of FM and AFM states are calculated according to the rectangular supercell shown in Fig. S1. Finally, after calculation, the J is 9.20 meV, and the $T_{\rm C}$ is 769 K. This result is higher than the room temperature, demonstrating that ScBrCl monolayer has the potential to be used in room temperature environments.

3.3. Electronic structure

Figure 2 shows the band structures of ScBrCl monolayer under different conditions. Without considering SOC, the band is completely spin polarized (see Fig. 2(a)). The valence band maximum (VBM) and conduction band minimum (CBM) of ScBrCl monolayer are located at Γ and M points, respectively, and this indicates an indirect bandgap with a bandgap value of 0.53 eV. At the same time, both the spin polarization directions in VBM and CBM are opposite, which indicates that ScBrCl monolayer is a bipolar magnetic semiconductor (BMS).[63,64] When considering SOC, VBM shifts to K point or K' point. We denote the valley polarization of the valence band as $\Delta_{\rm VB}$

$$\Delta_{\rm VB} = E_K^{\rm VB} - E_{K'}^{\rm VB}. \tag{6}$$

Among them, $E_K^{\rm VB}$ and $E_{K'}^{\rm VB}$ represent the energy extremes of the K and K' points in the valence band, respectively. When the time-reversal symmetry is broken, the valley polarization can be realized. For in-plane magnetization, there is no prominent valley polarization, as confirmed in Fig. 2(b). Next, we assume that the magnetization of ScBrCl monolayer is along $+z$ direction, resulting in a $\Delta_{\rm VB}$ of 44 meV (see Fig. 2(c)). As plotted in Fig. 2(d), the valley polarization and spin can be reversed by flipping the magnetization. Thus, both the spin and valley properties are related to the direction of magnetization. It provides the possibility of manipulating the magnetization axis to change the spin polarization at K/K' points.

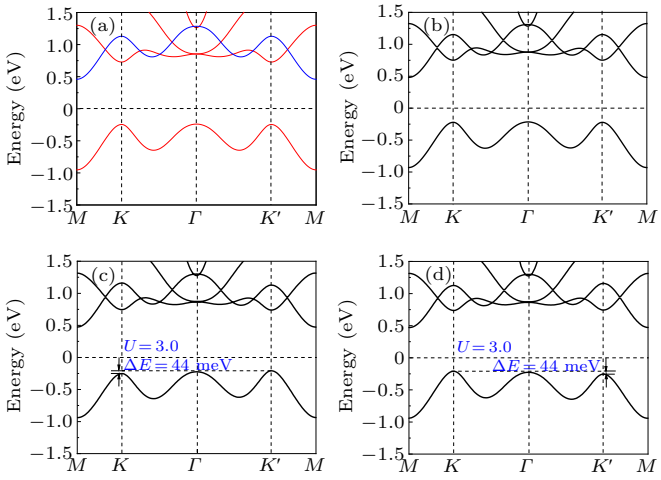


Fig. 2. (a) The band structure of ScBrCl monolayer without SOC. The red and blue bands represent the spin-up and spin-down states, respectively. (b)–(d) Considering SOC effect, the band structures of ScBrCl monolayer with different magnetic moment directions are shown, and the three band maps represent the magnetization of Sc atom along the $+x$, $+z$, and $-z$ directions, respectively.

According to Fig. 3(a), the valleys in the valence band are primarily from Sc-3d$_{xy}$ and Sc-3d$_{x^2-y^2}$ orbitals, but the valleys in the conduction band (local extreme value) are mainly dominated by Sc-3d$_{z^2}$ orbital. In order to further describe the principle of the valley polarization in ScBrCl monolayer, we will establish a simple model to illustrate its essence with the help of perturbation theory. The Hamiltonian of SOC can be written as $\hat{H}_{\rm SOC} = \lambda\hat{L}\cdot\hat{S} = \hat{H}^0_{\rm SOC} + \hat{H}^1_{\rm SOC}$, where λ refers to the coupling constant. We found that the states around the valley are mainly derived from the same spin channels, which are caused by spin polarization. A further result is that the interaction between the different spin states disappears, so the second term $\hat{H}^1_{\rm SOC} = 0$. So the Hamiltonian is obtained as[65]

$$\begin{aligned}\hat{H}^0_{\rm SOC} &= \alpha\hat{L}\cdot\hat{S} \\ &= \lambda\hat{S}_{z'}\left(\hat{L}_z\cos\theta + \frac{1}{2}\hat{L}_+ e^{-i\phi}\sin\theta + \frac{1}{2}\hat{L}_- e^{+i\phi}\sin\theta\right).\end{aligned} \tag{7}$$

In the above equation, $\hat{S}_{z'}$ and $\hat{L}_z$ represent the spin and orbital angular momentum operators of the z'/z component, respectively. To clearly determine the direction of the spin, we introduce the polar angle θ and the azimuth angle ϕ. And $\hat{L}_\pm = \hat{L}_x \pm \mathrm{i}\hat{L}_y$. Considering the contribution of the orbit to the band edge and the wave vector symmetry of the two valleys, we choose the basis functions $|\psi_c^\tau\rangle = |\mathrm{d}_{z^2}\rangle$ and $|\psi_v^\tau\rangle = (|\mathrm{d}_{x^2-y^2}\rangle + \mathrm{i}\tau|\mathrm{d}_{xy}\rangle)/\sqrt{2}$. In these two formulas, the valley index corresponding to K/K' valleys is expressed by τ, and $\tau = \pm 1$. The valence and conduction bands can be distinguished by subscripts v and c, respectively. In addition, valley polarization at the CBM and VBM can be given by the following formula:[66] $E_v^\tau = \langle\psi_v^\tau|\hat{H}^0_{\mathrm{SOC}}|\psi_v^\tau\rangle$ and $E_c^\tau = \langle\psi_c^\tau|H^0_{\mathrm{SOC}}|\psi_c^\tau\rangle$, respectively. For $\theta = 0$, that is, when the magnetic moment direction is along the $+z$ direction, equation (7) can be simplified as $\hat{H}^0_{\mathrm{SOC}} = \lambda\hat{S}_{z'}\hat{L}_z = \alpha\hat{L}_z$. Therefore,

$$E'_{\mathrm{C}} - E_{\mathrm{C}} = 0, \tag{8}$$

$$E'_{\mathrm{V}} - E_{\mathrm{V}} = \mathrm{i}\langle \mathrm{d}_{x^2-y^2}|\hat{H}^0_{\mathrm{SOC}}|\mathrm{d}_{xy}\rangle - \mathrm{i}\langle \mathrm{d}_{xy}|\hat{H}^0_{\mathrm{SOC}}|\mathrm{d}_{x^2-y^2}\rangle = 4\alpha, \tag{9}$$

in this calculation, we have used $L_z|\mathrm{d}_{xy}\rangle = -2\mathrm{i}|\mathrm{d}_{x^2-y^2}\rangle$ and $L_z|\mathrm{d}_{x^2-y^2}\rangle = 2\mathrm{i}|\mathrm{d}_{xy}\rangle$. Similarly, when the magnetization direction is along $-z$ direction, similar formulas $E'_{\mathrm{C}} - E_{\mathrm{C}} = 0$ and $E'_{\mathrm{V}} - E_{\mathrm{V}} = -4\alpha$ can easily be obtained. As a first-order perturbation in the SOC effect, the above analysis confirms that although valley degeneracy is eliminated in the VBM, but it still exists in the CBM, which is very consistent with first-principles calculations.

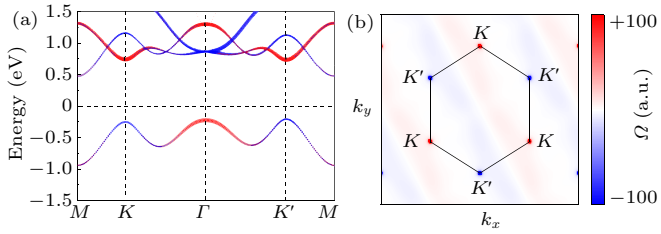


Fig. 3. (a) The orbital-resolved band structure of Sc atoms in ScBrCl monolayer with SOC, and the magnetization of Sc is along $+z$. The red and blue dots represent the d_{z^2} and $\mathrm{d}_{x^2-y^2}/\mathrm{d}_{xy}$ orbitals of Sc atoms, respectively. (b) The Berry curvature of ScBrCl monolayer when magnetization direction is along $+z$.

The ScBrCl monolayer is FVS material with 2D hexagonal lattice structure, which may produce anomalous Hall effect in the absence of an external magnetic field. Thus, we check the transport properties of ScBrCl monolayer with valley dependent properties. This transport property is closely associated to Berry curvature. For 2D structures, Berry curvature can be calculated using the following formula:[67,68]

$$\Omega_z(k) = -\sum_n \sum_{n\neq n'} f_n(k)\frac{2\,\mathrm{Im}\langle\psi_{nk}|\hat{v}_x|\psi_{n'k}\rangle\langle\psi_{n'k}|\hat{v}_y|\psi_{nk}\rangle}{(E_n - E_{n'})^2}. \tag{10}$$

In the above formula, f_n, Ψ_{nk}, and E_n refer to the equilibrium Fermi Dirac distribution function, the Bloch wave functions, and their eigenvalues, respectively. The velocity operators along different directions are represented by $\hat{v}_x$ and $\hat{v}_y$. We can see that the Berry curvatures of K/K' valleys are both nonzero and have different symbols, because of the presence of the abnormal velocity $v \propto -E \times \boldsymbol{\Omega}_Z$,[69] indicating that ScBrCl monolayer has opposite anomalous velocities at the two valleys. Due to the above properties, we can realize the anomalous valley Hall effect (AVHE) in ScBrCl monolayer. Through the method of hole doping, the Fermi level can be adjusted so that the Fermi level is between K/K' valleys, at which time the hole will stop at a valley. When the in-plane electric field is applied, Berry curvature causes the hole carrier to accumulate to one side of the sample, thus producing AVHE.

3.4. Strain effects and topological phase transition

The distance between magnetic and non-magnetic atoms or the distance between magnetic atoms in a material has a very obvious and important effect on various physical properties of the material. One of the reasons why 2D materials are so widely used is that they usually have much better tensile properties than their bulk counterparts.[70–73] For the above reasons, we continue to research the effect of strain on the electronic and magnetic properties of ScBrCl monolayer. Here, the biaxial strain (ε) is defined by

$$\varepsilon = \left(\frac{a - a_0}{a}\right) \times 100\%, \tag{11}$$

where a_0 and a represent the lattice constants of ScBrCl monolayer with and without strains, respectively. After calculation, it is proved that the ferromagnetic state of ScBrCl monolayer remains unchanged in the range of considered strain, as shown in Fig. S2. Next, we investigate the change of the band gap. Subsequently, we calculated the strain-dependent MAE of ScBrCl monolayers. As shown in Fig. 4(a), the calculated MAE becomes negative within the range of -6% to $+6\%$, indicating that the direction of magnetization is always along in-plane, but the MAE tends to 0 with the increase of tensile strain. Therefore, we can change the direction of magnetization by means of external magnetic field. Additionally, figure S3 plots the band structures when the magnetization direction is out-of-plane under different strain conditions. It is found that when the strain range is -6% to $+2\%$, the VBM and CBM of the band are located at different locations of K and M points in the Brillouin region, respectively. So ScBrCl monolayer is an indirect bandgap semiconductor in this range. When $3\% < \varepsilon < 6\%$, the VBM and CBM are located at K and K' points, and ScBrCl monolayer becomes a direct bandgap semiconductor. We mainly focus on the case of direct bandgap semiconductor. Figure 4(b) shows the variation of the respective bandgap values of K and K' valleys in this range.

Figure 5 shows the electronic structures of multiple magnetism-valley coupling (MVC) states in ScBrCl mono-

layer within diverse tensile strains. For unstrained system, the VBM of ScBrCl monolayer at the K' and K valleys comes from the Sc-3d$_{xy}$ and Sc-3d$_{x^2-y^2}$ orbitals, whereas its CBM comes from the Sc-3d$_{z^2}$ orbital. When the tensile strain is applied, the Sc-3d$_{xy}$ and Sc-3d$_{x^2-y^2}$ orbitals go upward, while the Sc-3d$_z^2$ orbital moves down. For $\varepsilon = 5.1\%$, one valley of the strained material shows semiconductor at the K valley, and the other indicates metallic character at the K' valley, which builds an intriguing HVM state, as shown in Fig. 5(b). It is worth noting that the HVM state has 100% valley polarization in valleytronics. On the other hand, due to incorporate the SOC effect, the HVM state with the same spin channel possesses 100% spin polarization.

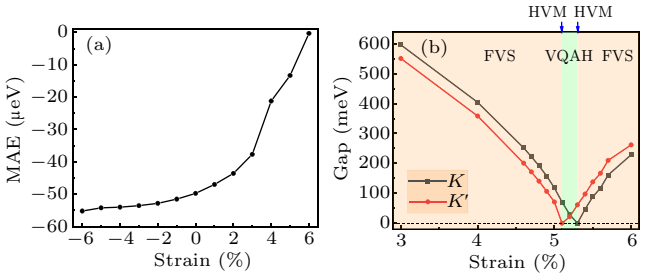


Fig. 4. (a) The variation of MAE with strains, (b) band gap and state phase diagram of K and K' valleys under tensile strain of ScBrCl monolayer.

When the tensile strain is continued to increase (see Fig. 5), the band gap of the K valley is got smaller. Furthermore, the band gap of the K' valley is reopened, resulting in one band inversion. Compared with original FV state, the orbital components are flipped in conduction band and valence band edges. As a consequence, one topological phase transition is occurred,[74,75] suggesting the existence of a quantum anomalous Hall (QAH) state[20,76] in this range. For the sake of verifying this guess, the $\varepsilon = 5.2\%$ is considered as an example. It can be clearly observed that the sign of $\Omega(k)$ in the K' valley reverses within this strain in contrast to unstrained system (Fig. 6(b)). The unit Chern number of $C = 1$ can be gained by the integration of $\Omega(k)$ in the first BZ. According to Fig. 6(d), a QAH insulator with one nonzero Chern number ($C = 1$) is confirmed by the quantized AHC ($\sigma_{xy} = Ce^2/h$).[77] It can be found that one single chiral edge state links the CBM and VBM within the bulk band gap. For $\varepsilon = 5.2\%$, the QAH state in ScBrCl monolayer is evidenced by these indicators. Hence, for this strained valleytronic material, the QAH phase can be expected to take place.

On the other hand, when the ε increases to +5.3%, the band gap at the K valley closes (Fig. 5(d)). Another HVM state is formed under this strain, which differs from the previous HVM state at 5.1% tensile strain, because it has a metal K valley and a semiconductor K' valley. When the strain continues to increase ($\varepsilon > 5.3\%$), another inversion occurs in the band composition, as shown in Fig. 5(j). Figures 6(a)–6(c) show that the Berry curvature has also undergone a sign reversal, that is, the signs of the Berry curvature of points K and K' valleys change from opposite sign to the same sign, which indicates a topological phase transition has occurred.[78] However, when the ScBrCl monolayer is stretched beyond 5.3% (Fig. 6(b)), the Berry curvature at points K and K' becomes the opposite sign again, showing trivial topology feature. In addition, as the strain increases, the band gap at the K valley reopens, at which point the Sc-3d$_z^2$ orbital occupies the VBM and the Sc-3d$_{xy}$ and Sc-3d$_{x^2-y^2}$ orbitals begin to occupy the CBM. This situation can be clearly shown by Fig. 5(j), the orbital component analysis diagram at 6% stretch. After the tensile strain exceeds 5.3%, ScBrCl monolayer returns to the ordinary FV state.

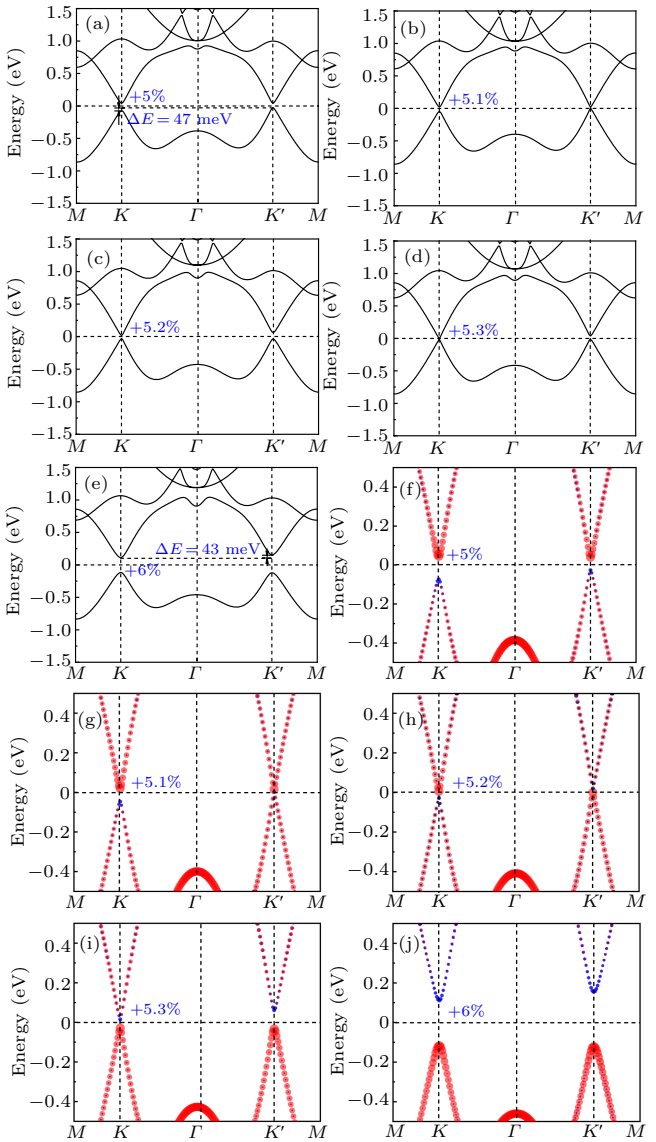


Fig. 5. (a)–(e) The strain value of 5%, 5.1%, 5.2%, 5.3%, and 6% of the energy band diagrams, respectively. (f)–(j) The corresponding orbit component analysis diagrams for ScBrCl monolayer.

To sum up, it can be seen that ScBrCl monolayer undergoes a series of topological transformations for $5.1\% < \varepsilon < 5.3\%$. As shown in Fig. 4(b), when ε is less than 5.1%, ScBrCl

monolayer is an FVS material. When $\varepsilon = 5.1\%$, ScBrCl monolayer changes to HVM, at which the band gap at K' point is closed. For $\varepsilon = 5.2\%$, the closed band gap reopens and ScBrCl monolayer transforms into a valley quantum anomalous Hall effect. When $\varepsilon = 5.3\%$, band gap in K point is closed, showing another HVM state. ScBrCl monolayer becomes FVS again for $\varepsilon > 5.3\%$. In addition, since ScBrCl monolayer is almost always valley polarized throughout the considered strain process, the previously discussed method for forming AVHE is still valid here.

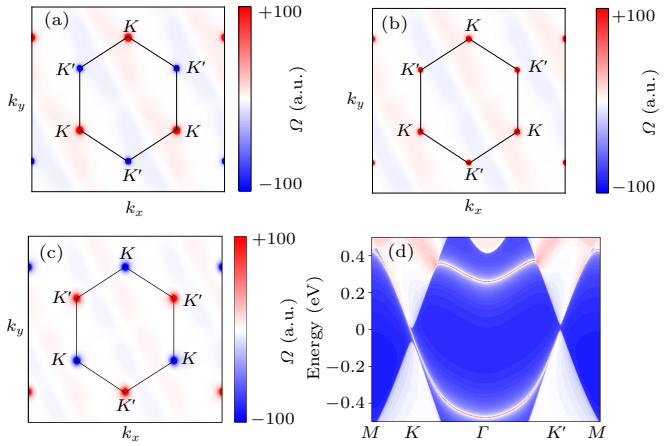


Fig. 6. The Berry curvature of ScBrCl monolayers under tensile strain sizes of (a) 5%, (b) 5.2%, and (c) 6%, respectively. (d) The edge state of ScBrCl monolayer under tensile strain of 5.2%.

4. Conclusion

We studied the physical properties of ScBrCl monolayer by using the first-principles calculations. Our results show that ScBrCl monolayer is a 2D FVS material, which has the following features: (i) ScBrCl monolayer has very high BKT transition temperature, good thermodynamic and kinetic stability. (ii) By changing the direction of magnetization from in-plane to out-of-plane, 44-meV great valley polarization and opposite Berry curvature can be generated, thus exhibiting AVHE feature. (iii) The strain can significantly regulate the valley properties of ScBrCl monolayer, and topological phase transition can be generated when the strain is stretched from 5.1% to 5.3%, showing the transition of FVS–HVM–VQAH–HVM–FVS states. This series of transformations can be confirmed by orbital composition inversion, Berry curvature, and, edge state, *etc*. In conclusion, our study broadens the application range of 2D FVS materials and is conducive to the practical application of ScBrCl monolayers.

Acknowledgement

Project supported by the National Natural Science Foundation of China (Grant No. 52173283).

References

[1] Han Y T, Ji W X, Wang P J, Li P and Zhang C W 2023 *Nanoscale* **15** 6830
[2] Fert A 2008 *Rev. Mod. Phys.* **80** 1517
[3] He R, Wang D, Luo N, Zeng J, Chen K Q and Tang L M 2023 *Phys. Rev. Lett.* **130** 046401
[4] Li S S, Ji W X, Hu S J, Zhang C W and Yan S S 2017 *ACS Appl. Mater. Interfaces* **9** 41443
[5] Wang Y P, Ji W X, Zhang C W, Li P, Zhang S F, Wang P J, Li S S and Yan S S 2017 *Appl. Phys. Lett.* **110** 213101
[6] Zhang M H, Zhang C W, Wang P J and Li S S 2018 *Nanoscale* **10** 20226
[7] Allen M J, Tung V C and Kaner R B 2010 *Chem. Rev.* **110** 132
[8] Zeng M, Xiao Y, Liu J, Yang K and Fu L 2018 *Chem. Rev.* **13** 6236
[9] Mak K F, Xiao D and Shan J 2018 *Nat. Photon.* **12** 451
[10] Luo J, Meng H, Xue X X, Chen K Q and Tang L M 2024 *Phys. Rev. B* **110** 085401
[11] Li Q, Chen K Q and Tang L M 2020 *Phys. Rev. Appl.* **13** 014064
[12] Xiao D, Yao W and Niu Q 2007 *Phys. Rev. Lett.* **99** 236809
[13] Yamamoto M, Shimazaki Y, Borzenets I V and Tarucha S 2015 *J. Phys. Soc. Jpn.* **84** 121006
[14] Sui M, *et al*. 2015 *Nat. Phys.* **11** 1027
[15] Mak K F, McGill K L, Park J and McEuen P L 2014 *Science* **344** 1489
[16] Gorbachev R V, *et al*. 2014 *Science* **346** 448
[17] Xiao D, Liu G B, Feng W, Xu X and Yao W 2012 *Phys. Rev. Lett.* **108** 196802
[18] Wang Y Z, Yang W, Zhang H and Xu X 2024 *Chin. Phys. B* **33** 17306
[19] Zhao J J, Liu G B, Chen P, Yao Y G, Zhang G Y and Du L J 2024 *Chin. Phys. Lett.* **41** 066801
[20] Pan H, Li Z, Liu C C, Zhu G, Qiao Z and Yao Y 2014 *Phys. Rev. Lett.* **112** 106802
[21] Zhou T, Zhang J, Jiang H, Žutić I and Yang Z 2018 *npj Quantum Mater.* **3** 39
[22] Hu H, Tong W Y, Shen Y H, Wan X and Duan C G 2020 *npj Comput. Mater.* **6** 129
[23] Hu C S, Wu Y J, Liu Y S, Fu S, Cui X N, Wang Y H and Zhang C W 2023 *Chin. Phys. B* **32** 037306
[24] Sun H, Li S S, Ji W X and Zhang C W 2022 *Phys. Rev. B* **105** 195112
[25] Zeng H, Dai J, Yao W, Xiao D and Cui X 2012 *Nat. Nanotechnol.* **7** 490
[26] Mak K F, He K, Shan J and Heinz T F 2012 *Nat. Nanotechnol.* **7** 494
[27] Aivazian G, *et al*. 2015 *Nat. Phys.* **11** 148
[28] Xu L, Yang M, Shen L, Zhou J, Zhu T and Feng Y P 2018 *Phys. Rev. B* **97** 041405
[29] Lu H Z, Yao W, Xiao D and Shen S Q 2013 *Phys. Rev. Lett.* **110** 016806
[30] MacNeill D, Heikes C, Mak K F, Anderson Z, Kormányos A, Zólyomi V, Park J and Ralph D C 2015 *Phys. Rev. Lett.* **114** 037401
[31] Zhang T, Ma Y, Xu X, Lei C, Huang B and Dai Y 2020 *J. Phys. Chem. C.* **124** 20598
[32] Norden T, Zhao C, Zhang P, Sabirianov R, Petrou A and Zeng H 2019 *Nat. Commun.* **10** 4163
[33] Zhang Q, Yang S A, Mi W, Cheng Y and Schwingenschlögl U 2016 *Adv. Mater.* **28** 959
[34] Huang B, *et al*. 2017 *Nature* **546** 270
[35] Sheng K, Zhang B, Yuan H K and Wang Z Y 2022 *Phys. Rev. B* **105** 195312
[36] Cheng H X, Zhou J, Ji W, Zhang Y N and Feng Y P 2021 *Phys. Rev. B* **103** 125121
[37] Luo C, Peng X, Qu J and Zhong J 2020 *Phys. Rev. B* **101** 245416
[38] Liu P, Liu S, Jia M, Yin H, Zhang G, Ren F, Wang B and Liu C 2022 *Appl. Phys. Lett.* **121** 063103
[39] Huang B, Liu W Y, Wu X C, Li S Z, Li H, Yang Z and Zhang W B 2023 *Phys. Rev. B* **107** 045423
[40] Guo S D, Wang M X, Tao Y L and Liu B G 2023 *Phys. Chem. Chem. Phys.* **25** 796
[41] Kohn W and Sham L J 1965 *Phys. Rev.* **140** A1133
[42] Hohenberg P and Kohn W 1964 *Phys. Rev.* **136** B864
[43] Kresse G and Furthmüller J 1996 *Phys. Rev. B* **54** 11169
[44] Kresse G and Furthmüller J 1996 *Comput. Mater. Sci.* **6** 15
[45] Perdew J P, Burke K and Ernzerhof M 1996 *Phys. Rev. Lett.* **77** 3865
[46] Perdew J P, Burke K and Ernzerhof M 1998 *Phys. Rev. Lett.* **80** 891
[47] Liechtenstein A I, Anisimov V I and Zaanen J 1995 *Phys. Rev. B* **52** R5467
[48] Dudarev S L, Botton G A, Savrasov S Y, Humphreys C J and Sutton A P 1998 *Phys. Rev. B* **57** 1505

[49] Togo A and Tanaka I 2015 *Scr. Mater.* **108** 1

[50] Gonze X and Lee C 1997 *Phys. Rev. B* **55** 10355

[51] Baroni S, de Gironcoli S, Dal Corso A and Giannozzi P 2001 *Rev. Mod. Phys.* **73** 515

[52] Bucher D, Pierce L C T, McCammon J A and Markwick P R L 2011 *J. Chem. Theory Comput.* **7** 890

[53] Kim H J, Li C, Feng J, Cho J H and Zhang Z 2016 *Phys. Rev. B* **93** 041404

[54] Mostofi A A, Yates J R, Lee Y S, Souza I, Vanderbilt D and Marzari N 2008 *Comput. Phys. Commun.* **178** 685

[55] Marzari N, Mostofi A A, Yates J R, Souza I and Vanderbilt D 2012 *Rev. Mod. Phys.* **84** 1419

[56] Wu Q, Zhang S, Song H F, Troyer M and Soluyanov A A 2018 *Comput. Phys. Commun.* **224** 405

[57] Mostofi A A, Yates J R, Pizzi G, Lee Y S, Souza I, Vanderbilt D and Marzari N 2014 *Comput. Phys. Commun.* **185** 2309

[58] Zhang J, *et al*. 2017 *ACS Nano* **11** 8192

[59] Andrew R C, Mapasha R E, Ukpong A M and Chetty N 2012 *Phys. Rev. B* **85** 125428

[60] Sheng K, Chen Q, Yuan H K and Wang Z Y 2022 *Phys. Rev. B* **105** 075304

[61] Jiang P, Kang L, Li Y L, Zheng X, Zeng Z and Sanvito S 2021 *Phys. Rev. B* **104** 035430

[62] Zhang S, Xu R, Duan W and Zou X 2019 *Adv. Funct. Mater.* **29** 1808380

[63] Wu Y, Sun W, Liu S, Wang B, Liu C, Yin H and Cheng Z 2021 *Nanoscale* **13** 16564

[64] Li X, Wu X, Li Z, Yang J and Hou J G 2012 *Nanoscale* **4** 5680

[65] Whangbo M H, Gordon E E, Xiang H, Koo H J and Lee C 2015 *Acc. Chem. Res.* **48** 3080

[66] Tong W Y, Gong S J, Wan X and Duan C G 2016 *Nat. Commun.* **7** 13612

[67] Yao Y, Kleinman L, MacDonald A H, Sinova J, Jungwirth T, Wang D S, Wang E and Niu Q 2004 *Phys. Rev. Lett.* **92** 037204

[68] Thouless D J, Kohmoto M, Nightingale M P and den Nijs M 1982 *Phys. Rev. Lett.* **49** 405

[69] Xiao D, Chang M C and Niu Q 2010 *Rev. Mod. Phys.* **82** 1959

[70] Liu C, Fu B, Yin H, Zhang G and Dong C 2020 *Appl. Phys. Lett.* **117** 103101

[71] Liu P, Zhang G, Yan Y, Jia G, Liu C, Wang B and Yin H 2021 *Appl. Phys. Lett.* **119** 102403

[72] Liu C, Wang B, Jia G, Liu P, Yin H, Guan S and Cheng Z 2021 *Appl. Phys. Lett.* **118** 072902

[73] Liu S, Yin H, Singh D J and Liu P F 2022 *Phys. Rev. B* **105** 195419

[74] Guo X S and Guo S D 2023 *Phys. Chem. Chem. Phys.* **25** 18577

[75] Qi X L and Zhang S C 2011 *Rev. Mod. Phys.* **83** 1057

[76] Zhou J, Sun Q and Jena P 2017 *Phys. Rev. Lett.* **119** 046403

[77] Wu B, Song Y L, Ji W X, Wang P J, Zhang S F and Zhang C W 2023 *Phys. Rev. B* **107** 214419

[78] Zhang S J, Zhang C W, Zhang S F, Ji W X, Li P, Wang P J, Li S S and Yan S S 2017 *Phys. Rev. B* **96** 205433